Effects of particle size on thermal decomposition of CL-20

Chongwei An*†, Xiaoheng Geng**, Jingyu Wang*, and Wenzheng Xu*

*Chemical Industry and Ecology Institute, North University of China, Taiyuan, Shanxi 030051 CHINA
 Phone : +86 03513922140
†Corresponding address : acw98081b1@163.com

**Urban and Environmental Science Department, Binzhou University, Binzhou, Shandong 256600 CHINA

Abstract

Three Hexanitrohexaazaisowurtzitane (CL-20) samples with different particle size are prepared and tested by means of differential scanning calorimetry (DSC). Scanning Electron Microscope (SEM), laser granularity measurement and X-ray diffraction (XRD) were employed to characterize the CL-20 samples. The kinetic parameters, reaction rate constant, thermal stability and thermodynamic parameters of CL-20 samples were studied and contrasted. Results show that the mean particle size of three CL-20 samples is 56.73μm, 6.86μm and 0.76μm, respectively. The ε-phase purity of raw CL-20, micron CL-20 and submicron CL-20 is calculated as 96.9%, 96.0% and 94.8%, respectively. The peak temperature, activation energy, thermal stability and thermodynamic parameters of CL-20 are all decreasing with the reduction of particle size.

1. Introduction

Hexanitrohexaazaisowurtzitane (HNIW or CL-20) - a high energy material (HEM) with cage structure, is considered as the most powerful explosive today. CL-20-based compositions provide significantly greater energy and higher density than similar HMX-based compositions. CL-20-based formulations are being developed and evaluated in explosive, rocket, and gun propellant applications[1,2]. It is reported that the density and heat of formation of CL-20 is 2.04 g·cm^{-3} and about +419 kJ·mol^{-1}, respectively[3]. Due to its superior performance, it gained significant interest in the recent past.

Thermal decomposition properties are tied up with some properties of explosives, such as shelf life, thermal stability, compatibility and ballistic trajectory performance. The thermal decomposition of explosives based on DSC, DTA and TG data have been carried out for several years[4,5]. Kinetic studies have played an important role in thermal analysis, in which the main purpose is to determine the mechanism of pyrolysis reaction and to calculate the parameters of the Arrhenius equation. These data are required for energetic materials

to be qualified for performance and safety in their manufacture, handling, storage and use[6]–[8]. Many factors such as crystal size and size distribution, crystal phase and crystal defects, affect the thermal decomposition of explosive[8]–[10]. Recently, the relation between crystal properties and thermal decomposition of CL-20 has been given an initial study. V. V. Nedelko and his coworkers investigated the thermal decomposition kinetics of different polymorphs of CL-20 (α, γ and ε) by thermogravimetry. They found that thermal decomposition increases in the series : $\alpha < \gamma < \varepsilon$ and the thermal decomposition properties depended on the mean size and the size distribution of the crystals for the same polymorph[11]. In 1999, J.H. Jim studied the influence of the particle size on the thermal decomposition of ε-CL-20 and found that the thermal kinetic parameters such as activation energy (E) and pre-exponential factor (A) depended little on the particle size of ε-HNIW in the range 4-180μm[12]. However, it is not a complete and systematic study, which doesn't cover the submicron particles. Moreover, few investigations have been done on the thermal decomposition of submicron CL-20. Herein, the

thermal decomposition of CL-20 with 56.73 µm, 6.86 µm and 0.76 µm mean particle size is investigated by means of differential scanning calorimetry (DSC). Also, the thermal kinetic parameters, thermodynamic parameters and thermal stability of CL-20 samples are surveyed and contrasted systematically.

2. Experimental
2.1 Materials

CL-20 (purity=99.9%) is provided by Beijing Institute of Technology of China; ethyl acetate (AR) and normal heptane (AR) are purchased from Tianjin Tianda Chemical Industry Co. Ltd. of China. a-Al_2O_3(purity $\geq$ 99.9%, 1-5 μm), was perchased from Shandong Zibo Jiezhong new material limited company, China.

2.2 Preparation of fine CL-20

The micron and submicron CL-20 are prepared by solvent - nonsolvent method. At first, the raw CL-20 is highly dissolved in acetic ether at 60°C, and then the solution is added into normal heptane to induce the crystallization at 25°C. Finally, the crystalline powders are filtered by a vacuum filter and dried in a vacuum freeze drier.

In this process, two important factors: the dropping rate of solution and mixing speed, affect the particle size of CL-20. When they are 5 ml·min^{-1} and 500 r·min^{-1}, the micron CL-20 is obtained. While, the submicron CL-20 is prepared at the dropping rate of 2 ml·min^{-1} and the mixing speed of 1000 r·min^{-1}

2.3 Characterization of CL-20 with different size

The profiles and size of CL-20 are characterized by S-4700 Scanning Electronic Microscope made by Hitachi Corporation, Japan. Particle size and size distribution of CL-20 are also measured with a BI-90PLUS laser particle sizer made by Brookhaven Instruments Corporation, USA.

The phase purity of CL-20 samples was determined by X-ray diffraction (XRD) analysis on the Rigaku D/MAX-RB diffractometer equipped with a graphite diffracted-beam monochromator. CuKa radiation (40 kV, 100 mA) was used. The 2θ range was from 10° to 80° at a scanning speed of 0.02° ·s^{-1}.

2.4 DSC test

The DSC experiments are carried out with DSC131 instrument made by Setaram Co., France. The conditions of DSC are as follows: sample mass, 0.7 mg; heating rate, 5, 10, 20°C·min^{-1}; N$_2$ atmosphere (30 mL·min^{-1}); aluminum cell with pierced lid.

3. Results and discussions
3.1 Characterization of CL-20 samples
3.1.1 SEM analysis

Figure 1 provides SEM images of CL-20 powders of different particle sizes. The raw CL-20 (Figure 1a) is polyhedron morphology and its particle size is about 20-150 µm. SEM images of Figure 1b and Figure 1c show that by solvent-nonsolvent process, the particle morphology of
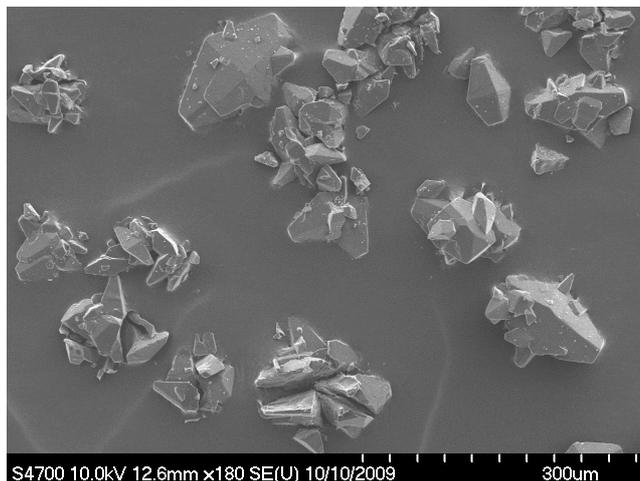
Figure 1a
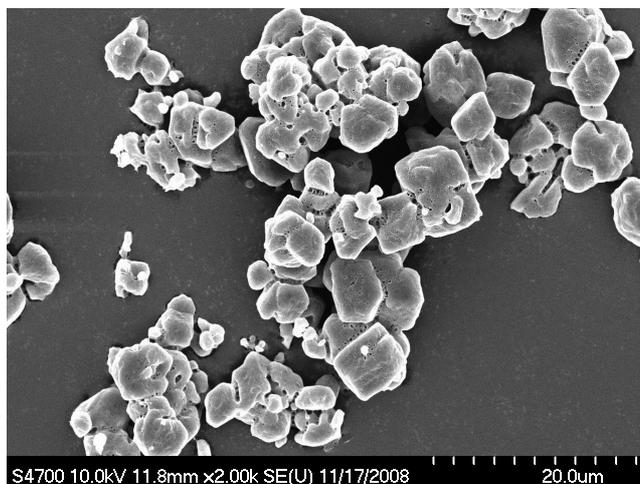
Figure 1b
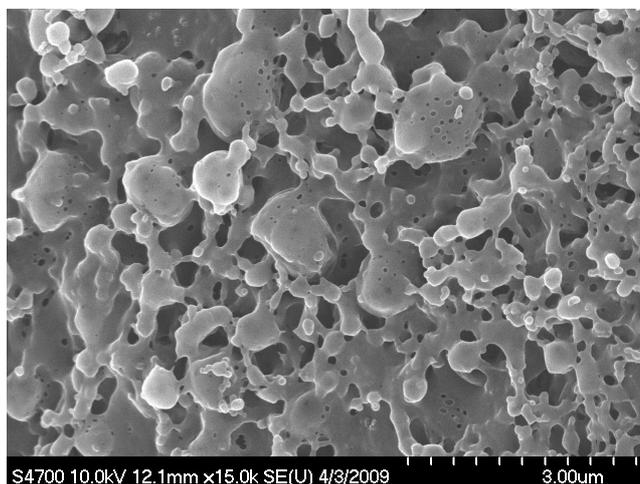
Figure 1c

Figure 1   SEM images of CL-20 with different particle size, a: raw CL-20; b: Micron CL-20; c: Submicron CL-20.

both CL-20 samples become nearly globular, however, their particle sizes are reduced to 3-10 µm and 0.5-0.8 µm, respectively. It is obvious that there are differences in particle size among the three kinds of samples.
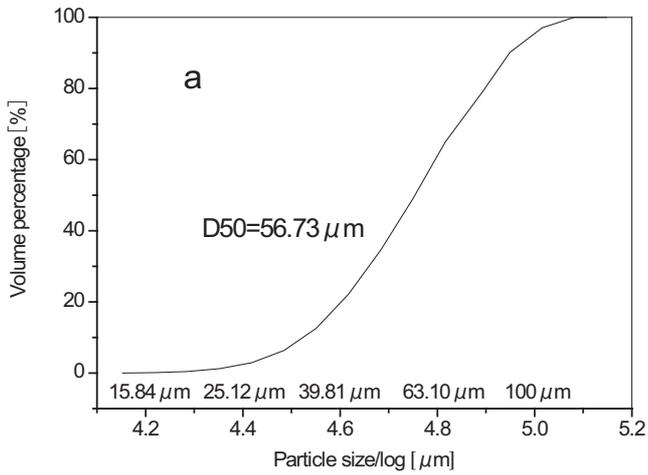
Figure 2a
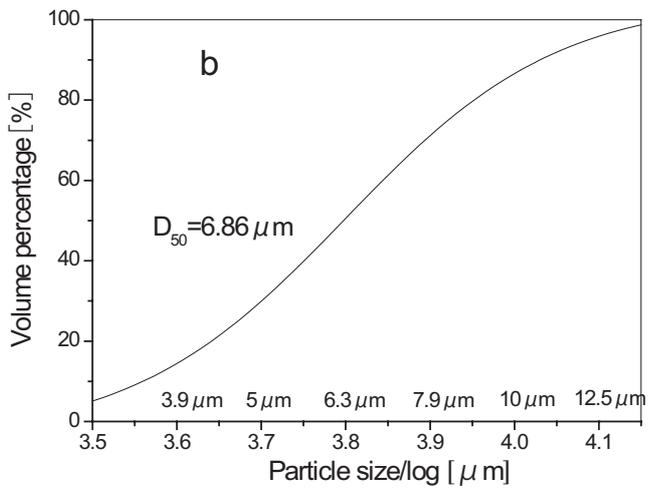
Figure 2b
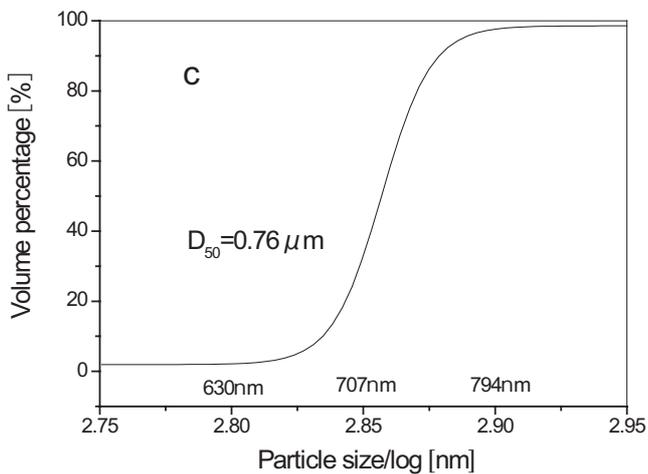
Figure 2c

Figure 2 Particle size and size distribution of CL-20 samples, a: raw CL-20; b: Micron CL-20; c: Submicron CL-20.

3.1.2 Particle size analysis

Figure 2 shows the curves and data of particle size and size distribution of three CL-20 samples. In Figure 2a, it can be seen that the size cumulative distribution of raw CL-20 is broader and its mean particle size is 56.73 μm. Figure 2b shows that the size distribution of micron CL-20
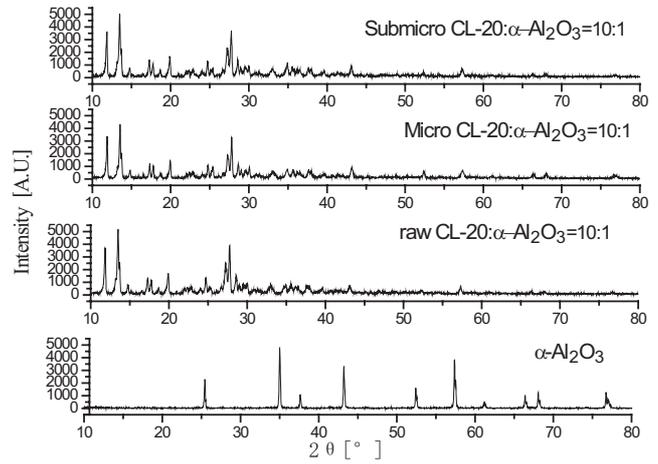
Figure 3 XRD patterns of α-Al_2O_3 and the mixture of α-Al_2O_3 and CL-20 samples.

is about from 3um to 13 μm and the mean particle size is 6.86 μm. The curve in Figure 2c indicates that the submicron CL-20 with 0.76 μm mean particle size has a narrower size distribution. These results are in accordance with the SEM results.

3.1.3 XRD analysis

It has been reported that ε-CL-20 exhibits a unique non-overlapping diffraction peak at 19.9° 2θ in the XRD patterns. Moreover, the characteristic peak intensity ratio of ε-CL-20 to α-Al_2O_3 is proportional to their weight ratio[13]. Therefore, α-Al_2O_3 is selected as the reference material to determine the phase purity of CL-20 according to XRD data. The XRD patterns of α-Al_2O_3 and the mixture of α-Al_2O_3 and CL-20 samples are shown in Figure 3.

From Figure 3, it is found that the XRD patterns of the three mixtures of α-Al_2O_3 and CL-20 samples are similar in shape and peak intensity, implying that the three CL-20 samples have the similar ε-phase purity. Following the quantitative method reported by the literature[13], the ε-phase purity raw CL-20, micron CL-20 and submicron CL-20 is calculated as 96.9%, 96.0% and 94.8%, respectively.

3.2 Results of thermal analysis

Figure 4 shows the DSC thermographs of CL-20 with different size. It can be found that each DSC curve of CL-20 has an exothermic peak, which is attributed to the self-decomposition of CL-20. In each case, the peak temperature increases with the increase of heating rate. In addition, at the same heating rate, the peak temperature decreases with decreasing the particle size of CL-20.

3.3 Thermal kinetic parameters

The decomposition kinetic parameters of three CL-20 samples are determined via Kissinger (1)and Ozawa (2) method[8), 15)].

$$\ln\frac{\beta_i}{T_{pi}^2} = \ln\frac{AR}{E} - \frac{E}{RT_{pi}} \qquad (1)$$

$$\log\beta_i + 0.496\frac{E}{RT_{pi}} = C \qquad (2)$$
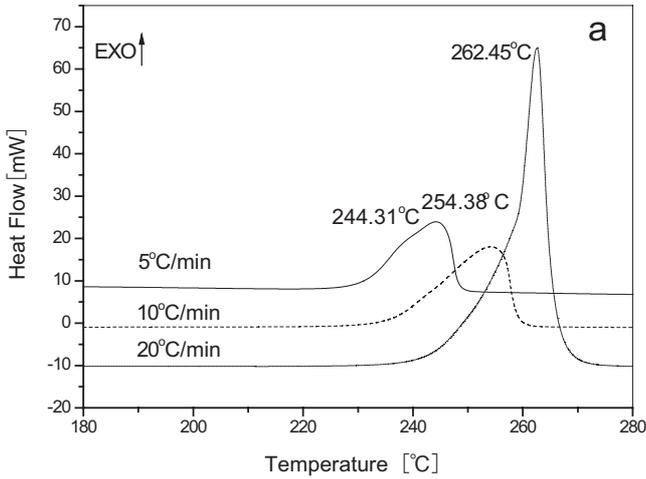
Figure 4a
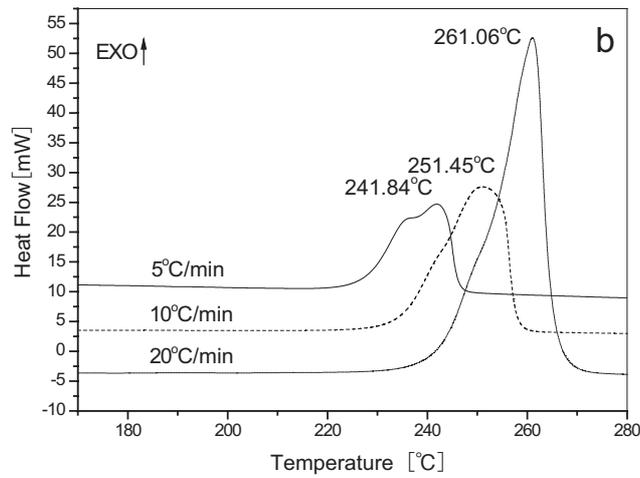
Figure 4b
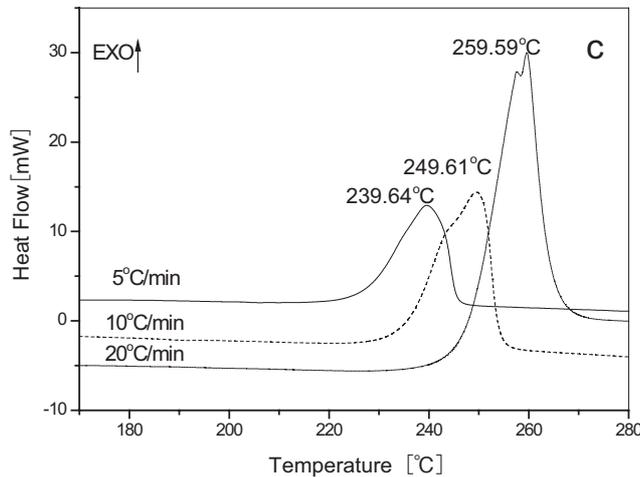
Figure 4c

Figure 4   DSC thermographs of CL-20 with different size at 5,10, 20°C/min heating rate. a: raw CL-20; b: micron CL-20; c: submicron CL-20.

Where β_i is the heating rate in $K \cdot min^{-1}$; T_{pi} is the peak temperature of decomposition at β_i in K; A is the pre-exponential factor; E is the activation energy in $J \cdot mol^{-1}$; R is the universal gas constant, $8.314\ J \cdot mol^{-1} \cdot K^{-1}$.

For equation1,when $\ln(\beta_i/T^2)$ is plotted against $1/T_{pi}$, a straight line is obtained and shown in Figure 5. The activation energy (E_a) and the frequency factors (A) of CL-
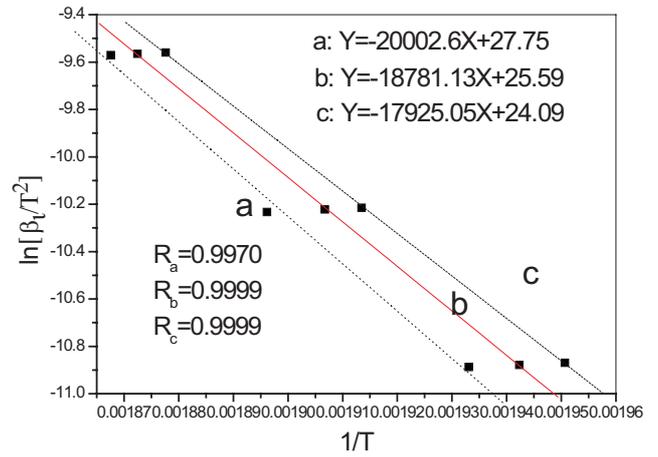
Figure 5   Kissinger's plots of $\ln(\beta_i/T^2)$ versus reciprocal peak temperature $1/T$ for CL-20 with different size. Symbol R is used to identify the linear correlation coefficient of $\ln(\beta_i/T^2)$ to$1/T$. a: raw CL-20; b: micron CL-20; c: submicron CL-20.
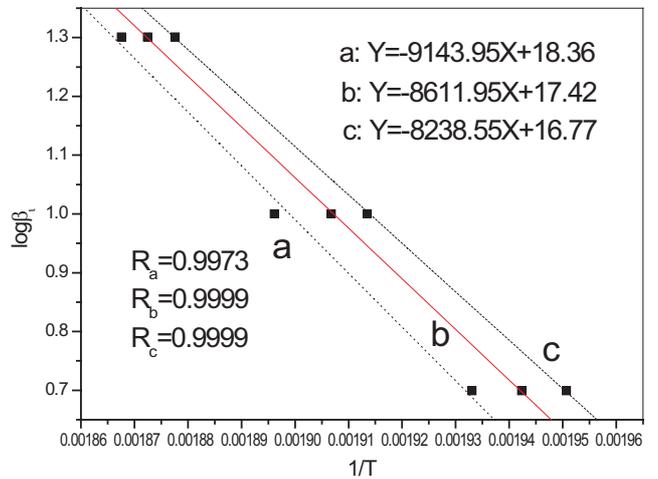
Figure 6   Ozawa's plots of $\log\beta_i$ versus reciprocal peak temperature $1/T$ for CL-20 with different size. Symbol R is used to identify the linear correlation coefficient of $\log\beta_i$ to $1/T$. a: raw CL-20; b: micron CL-20; c: submicron CL-20.

20 samples are calculated from the slope $-E/R$ and the intercept $\ln(AR/E)$. On the other hand, in equation 2, activation energy can be determined from the plots of the logarithm of the heating rate versus the inverse of the temperature at the maximum reaction rate in constant heating rate experiments. The plots of $\log(\beta_i)$ against $1/T$ for three CL-20 samples are shown in Figure 6.

From Figure 5 and Figure 6, the plots of both $\ln(\beta_i/T^2)$ and $\log\beta_i$ against $1/T$ for CL-20 samples are all straight lines with higher linear correlation coefficient. Thus, both Kissinger's and Ozawa's kinetic model provide a good description of the overall observed decomposition behavior in this temperature range. Moreover, it indicates that mechanisms of thermal decomposition of CL-20 with different particle sizes over this temperature range are consistent[16].

Based on these plots, the activation energy (E_a) and the frequency factors (A) of CL-20 samples are calculated and summarized in Table 1.

As is shown in Table 1, the activation energy calculated

Table 1 Thermal kinetic parameters of CL-20 samples by Kissinger and Ozawa method.

Samples	Method	Activation energy [kJ·mol^{-1}]	Frequency factor logA[s^{-1}]
Raw CL-20	Kissinger	166.30 (±0.3)	16.35 (±0.03)
	Ozawa	153.27 (±0.2)	15.01 (±0.05)
Micron CL-20	Kissinger	156.15 (±0.4)	15.39 (±0.02)
	Ozawa	144.35 (±0.4)	14.16 (±0.05)
Submicron CL-20	Kissinger	149.03 (±0.3)	14.71 (±0.04)
	Ozawa	138.09 (±0.5)	13.57 (±0.03)
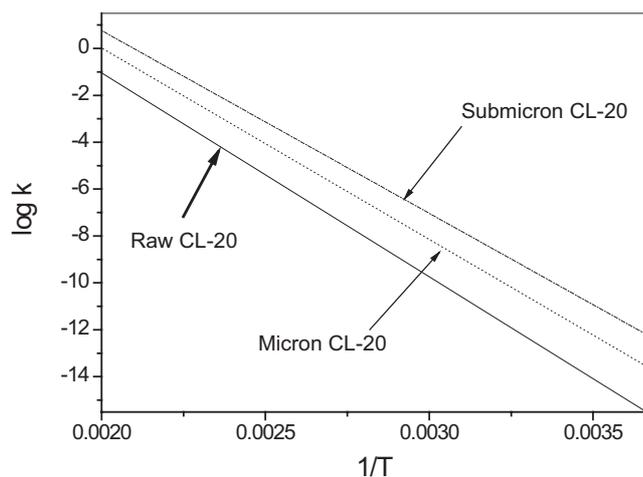
Figure 7 Plots of logk versus 1/T for three CL-20 samples.

by Kissinger method is about 10 kJ·mol^{-1} more than that of Ozawa method. The data in Table 1 implement that particle size has great influence on the thermal kinetic parameters. With the same calculated method, both activation energy and frequency factor decrease with particle size decreasing.

3.4 Thermal decomposition reaction rate constant

According to Arrhenius, the thermal decomposition reaction constant (k) of explosives can be determined by the following equation[16].

$$\log k = \log A - \frac{E}{2.3RT} \tag{3}$$

From Eq.(3), it can be found that logk has the linear function with 1/T, the slope and intercept is equal to E/2.3 R and logA, respectively. The plots of log k versus 1/T for the three CL-20 samples are shown in Figure 7.

As is shown in Figure 7, at the same temperature, submicron CL-20 has the highest logk value, the micron takes the second place, and the raw has the lowest logk.

3.5 Thermal stability

The thermal stability of an explosive is defined as the ability to keep the chemical properties from transforming under thermal action. It can be expressed by its critical explosion temperature (T_b), which is an important parameter required to insure safe storage and process

Table 2 Thermodynamic parameters for three CL-20 samples

samples	ΔS*[J·mol^{-1}·k^{-1}]	ΔH*[kJ·mol^{-1}]	ΔG*[kJ·mol^{-1}]
Raw CL-20	55.43	162.12	134.22
Micron CL-20	37.07	151.97	133.36
Submicron CL-20	24.07	144.87	132.82

operations involving explosives, propellants and pyrotechnics[17),18]. Tb can be calculated according to the data obtained from thermal analysis based on Eqs. (4) and (5).

$$T_e = T_{pi} - b\beta_i - c\beta_i^2 \tag{4}$$

$$\frac{E}{RT_b^2}(T_b - T_e) = 1 \tag{5}$$

Where β_i is the heating rate in K·min^{-1}; T_{pi} is the peak temperature of decomposition at β_i in K; T_e is the peak temperature when β_i is zero in K; b and c are constants; T_b is the self-ignition temperature in K; E is the activation energy in J·mol^{-1}; R is the universal gas constant, 8.314 J·mol^{-1}·K^{-1}.

For the raw, micron and submicron CL-20, T_e obtained from Eq. (3) is 230.22°C, 229.03°C and 227.42°C, respectively; the critical explosion temperature calculated by Eq. (4) is 243.78°C, 243.21°C and 241.20°C by using Kissinger data, respectively.

3.6 Thermodynamic parameters

The thermodynamic parameters for three CL-20 samples, i.e. activation entropy (ΔS*), activation enthalpy (ΔH*) and activation free energy (ΔG*), are obtained from the following equations[19), 20]. The computed results are tabulated in Table 2.

$$Ae^{-E/RT} = \frac{k_B T}{h}e^{-\Delta G*/RT} \tag{7}$$

$$\Delta H* = E - RT \tag{8}$$

$$\Delta G* = \Delta H* - T\Delta S* \tag{9}$$

Where k_B is Boltzmann constant, 1.3807×10^{-23}J·K^{-1}; h is Plank constant, 6.626×10^{-34}J·s^{-1}; T is T_e obtained by Eq. (4); A and E are the kinetic parameters calculated by Kissinger method.

From Table 2, it can be seen that ΔS*, ΔH* and ΔG* of CL-20 are all decreasing with particle size decreasing.

4. Conclusion

In this paper, the thermal decomposition of three CL-20 samples with different mean particle size (56.73μm, 6.86 μm and 0.76μm) are studied by DSC. By analyzing the DSC data, it is found that the particle size of CL-20 has some influences on the thermal decomposition. The peak temperature, activation energy, thermal stability and thermodynamic parameters of CL-20 are all decreasing with the reduction of particle size.

References

1) A.K. Mandal, C.S. Pant, S. M. Kasar, and T. Soman, J. Energ. Mater., 27, 231 (2009)

2) R.L. Simpson, P.A. Urtiew, and D.L. Ornellas, Propell. Explos. Pypot., 22, 249 (1997)

3) M. Geetha, U.R. Nair, D. B. Sarwade, G. M. Gore, and S. N, J. Therm. Anal. Calorim., 73, 913 (2003)

4) L.A. Ramos, E.T.G. Cavalheriro, and G.O. Chierice, J. Therm. Anal. Calorim., 79 : 49 (2005)

5) G. Singh, R. Prajapati, and R. Frohlich, J. Hazard. Mater., A 118, 75 (2005)

6) P.S. Kapoor, P. Srivastava, and G. Singh, J. Hazard. Mater., 150, 687 (2008)

7) S.M. Pourmortazavi, M. Fathollahi, S.S. Hajimirsadeghi, and S.G. Hosseini. Thermochim. Acta, 443, 129 (2006)

8) M.R. Sovizi, S.S. Hajimirsadeghi, and B. Naderizadehb. J. Hazard. Mater., 168, 1134 (2009)

9) M. Fathollahi, S.M. Pourmortazavi,S. and G. Hosseini, J. Energ. Mater., 26, 52 (2008)

10) X.L. Song, Y. Wang, C.W. An, X.D. Guo, and F.S. Li, J. Hazard. Mater., 159, 222 (2008).

11) V.V. Nedelko, N. V. Chukanov, A. V. Raevskii, B. L. Korsounskii, T. S. Larikova, and O. I. Kolesova, Propell. Explos. Pypot., 25, 255 (2000).

12) J.H. Jim, and Y. J. Yim, J. chem. Eng. Jpn, 32, 237 (1999)

13) H.X. Chen, S.S. Chen, L.J. Li, and S.H. Jin, Propell. Explos. Pypot., 33, 467 (2008)

14) M.F. Foltz, C. L. Coon, F. Garcia, and A. L. Nichols, Propell. Explos. Pypot., 19, 133 (1994)

15) H.E. Kissinger, Anal. Chem., 29, 1702 (1957)

16) A.S. Tompa, and R.F. Boswell, Thermochim. Acta., 357-358, 169 (2000)

17) T.L. Zhang, R.Z. Hu, Y. Xie, and F.P. Li, Thermochim. Acta., 244, 171 (1994)

18) R.Z. Hu, Z.Q. Yang, and Y.J. Liang, Thermochim. Acta., 134, 429 (1988)

19) J.M. Criado, L.A. Perez-Maqueda, and P.E. Sanchez-Jimenez, J. Therm. Anal. Calorim., 82, 671 (2005)

20) M.O. Humienik, and J. Mozejko, Thermochim. Acta., 344, 73 (2000)